BJRS
BRAZILIAN JOURNAL OF RADIATION SCIENCES

doi.org/10.15392/2319-0612.2024.2658
2024, 13(4B) | 01-28 | e2658
Submitted: 2024-08-28
Accepted: 2025-05-20

Computational Fluid Dynamics study of element type and turbulence model impact on a flow over a spacer grid using Simcenter STAR-CCM+

Vieira[a*], T. A. S.; Carvalho[b], Y.M.; Castro[b], H. F. P.; Carvalho[b], K. A.; Gonçalves[b], R. C.; Araújo[a], P. H.; Cury[b], D.; Silva[b], V. V. A.; Barros[b], G. P.; Santos[b], A. A. C.

[a]Siemens Digital Industries
[b]Centro de Desenvolvimento da Tecnologia Nuclear

[*]Correspondence: tiago.santiago-vieira@siemens.com

Abstract: This study presents a numerical investigation into the impact of various mesh element types on water flow results through a representative spacer grid, utilizing Computational Fluid Dynamics (CFD). The study evaluates the variations of the k−ϵ turbulence model available in Simcenter STAR-CCM+ across different mesh types. Three predominant cell types were employed: cartesian, polyhedral, and tetrahedral, alongside three k−ϵ models: Standard Two-layer (STL), Realizable Two-layer (RTL), and Elliptic Blending (EB). The analysis was conducted using a PWR vane-type spacer grid arranged in a 2x2 configuration. The findings demonstrated a strong correlation with experimental data available in the literature. However, the cartesian and tetrahedral meshes attenuated the velocity profiles post-spacer grid. The polyhedral mesh, in conjunction with the RTL and EB k−ϵ models, yielded results more closely aligned with the experimental data. Regarding Secondary Flow (SF), the results indicated a consistent trend of decreasing intensity downstream of the spacer grid. The Polyhedral EB and RTL models exhibited behavior most consistent with the experimental results.

Keywords: CFD, spacer grids, mesh analysis.

SBPR

BJRS
BRAZILIAN JOURNAL OF RADIATION SCIENCES

doi.org/10.15392/2319-0612.2024.2658
2024, 13(4B) | 01-28 | e2658
Submitted: 2024-08-28
Accepted: 2025-05-20

Estudo de CFD do impacto do tipo de elemento de malha e do modelo de turbulência no escoamento sobre uma grade espaçadora usando Simcenter STAR-CCM+

Resumo: Neste estudo, foi realizada uma investigação numérica sobre o efeito de diferentes tipos de elementos de malha nos resultados do escoamento de água através de uma grade espaçadora representativa, utilizando CFD (Computational Fluid Dynamics). Além disso, foram avaliadas as variações do modelo de turbulência k−ϵ disponíveis no Simcenter STAR-CCM+, utilizando diferentes tipos de malhas desenvolvidas. Foram utilizados três tipos de elementos dominantes (cartesiano, poliédrico e tetraédrico) e três modelos k−ϵ (Standard Two-layer – STL, Realizable Two-layer – RTL e Elliptic Blending – EB). Para a análise de desempenho, foi utilizada uma grade espaçadora do tipo aletada de um PWR em um arranjo 2x2. Os resultados demonstraram concordância com os dados experimentais disponíveis na literatura. No entanto, as malhas cartesiana e tetraédrica amorteceram os perfis de velocidade após a grade espaçadora. A malha poliédrica com os modelos k−ϵ RTL e EB apresentou resultados mais próximos aos experimentais. Em relação ao Secondary Flow (SF), os resultados mostraram consistência com a tendência de redução da intensidade a jusante da grade espaçadora. Os modelos poliédricos EB e RTL exibiram um comportamento aproximado aos resultados experimentais.

Palavras-chave: CFD, grades espaçadoras, análise de malhas.

SBPR

1. INTRODUCTION

The fuel assemblies are the main devices present in a Pressurized Water Rector (PWR) core. They are formed basically by fuel rod bundles with guide tubes between them, bottom and top nozzles and spacer grids. The spacer grids are components with two main functions: keeping the bundle assembled and promoting fluid mixing [2]. The second purpose increases flow turbulence in the subchannels of the referred structure. As a result, they not only maximize heat transfer through the fuel assemblies but also induce pressure drop. Therefore, its design holds significant aspects for efficiency of the system [3].

Computational Fluid Dynamics (CFD) calculations have been performed to comprehend the impact of spacer grids on water flow through the fuel assemblies [4, 5, 6, 7]. To implement this approach, it is necessary to discretize the domains (mesh generation) under study. This discretization needs to be suitable for the desired application, considering that the quality of the mesh directly affects the accuracy of the results. During the mesh creation process, the type of element to be used must be defined, which will determine the geometry of the domain cells.

Different mesh element types in CFD simulations are crucial as they influence the accuracy, stability, and computational efficiency of the simulations. Various mesh elements, such as hexahedra, tetrahedra, and polyhedral, can better capture the geometry and flow characteristics of different regions within the simulation. For instance, hexahedral elements are often preferred for their accuracy in Cartesian grids. The choice of mesh elements affects computational cost. Cartesian meshes with hexahedral elements are computationally efficient for simple geometries, while unstructured meshes with tetrahedral or polyhedral elements offer greater flexibility for complex geometries. Tetrahedral meshes provide great flexibility in meshing intricate geometries and adapting to local flow features, but they can be less

efficient computationally. Polyhedral meshes combine the benefits of both Cartesian and tetrahedral grids, offering better accuracy by reducing numerical diffusion and capturing flow features more effectively.

In [8] assessed the impact of different spacer grid vanes configuration. In a subsequent work, [9] showed a possibility to reduce the domain from a 5x5 to a 2x2 rods. This allowed the usage of more refined meshes and the evaluation of the refinement level impact on the results. The referred works were performed using tetrahedral meshes. However, cartesian and polyhedral meshes might possibly exhibit advantages for simulations of this kind of flow since they are less demanding computationally [10, 11].

[12] validated a model developed using Simcenter STAR-CCM+ [1] for a vane type 5x5 fuel bundle using a polyhedral mesh. They evaluated several turbulence models, with $k-\epsilon$ presenting better agreement with the measurements. Still using Simcenter STAR-CCM+ [1] and $k-\epsilon$ turbulence model, [13] validated a vane type spacer grid using a 5x5 model, but implementing cartesian mesh.

The $k-\epsilon$ models provide a good compromise between robustness, computational cost, and accuracy. They are generally well suited to industrial-type applications that contain complex recirculation, with or without heat transfer.

The $k-\epsilon$ turbulence model holds significant importance in CFD simulations owing to its robustness, simplicity, and accuracy across a diverse spectrum of turbulent flow conditions. The $k-\epsilon$ model is particularly effective in predicting mean flow characteristics and handling complex flow phenomena, such as boundary layer separation and recirculation, as is the case for the flow around fuel bundles with vane-type spacer grids. Its semi-empirical nature, based on phenomenological considerations and empirical data, ensures that it can be applied to diverse industrial scenarios with reliable results. Regarding turbulence modeling, the $k-\epsilon$ turbulence model is a two-equation model that solves transport equations for the

turbulent kinetic energy (k) and the turbulent dissipation rate (ϵ) to ascertain the turbulent eddy viscosity. Several versions of the $k-\epsilon$ model have been in use for many decades, and it has emerged as the most extensively used model for industrial applications. Since the inception of the $k-\epsilon$ model, there have been innumerable attempts to refine it. The most substantial improvements have been integrated into Simcenter STAR-CCM+ [1].

The original $k-\epsilon$ turbulence model by [14] was implemented with wall functions. This high Reynolds number approach was subsequently modified to account for the blocking effects of the wall (viscous and buffer layer) using a low Reynolds number approach and a two-layer approach.

The two-layer approach, initially proposed by [15], enables the $k-\epsilon$ model to be applied in the viscous-affected layer (including the viscous sub-layer and the buffer layer). In this approach, the computation is bifurcated into two layers. In the layer adjacent to the wall, the turbulent dissipation rate and the turbulent viscosity are specified as functions of wall distance. The values specified in the near-wall layer are smoothly blended with the values computed from solving the transport equation far from the wall. The equation for the turbulent kinetic energy is solved across the entire flow domain. This explicit specification is arguably no less empirical than the damping function approach, and the results are often as good or better.

The Realizable $k-\epsilon$ model incorporates a new transport equation for the turbulent dissipation rate [16]. Additionally, a variable damping function (f_μ) expressed as a function of mean flow and turbulence properties is applied to a critical coefficient of the model (C_μ). This procedure enables the model to satisfy certain mathematical constraints on the normal stresses consistent with the physics of turbulence (realizability). This concept of a damped C_μ is also consistent with experimental observations in boundary layers.

The Standard Two-layer (STL) and the Realizable Two-Layer (RTL) $k-\epsilon$ models combines those initial $k-\epsilon$ models with the two-layer approach. The coefficients in the models are identical, but the model gains the added flexibility of an all-wall treatment.

The STL model and the RTL k−ϵ models offer the most mesh flexibility. They can be used with the same meshes as the high Reynolds number versions. They give good results on fine meshes (that is, low Reynolds number type or low y+ meshes), and produce the least inaccuracies for intermediate meshes (that is, 1<y+<30) [1].

The Elliptic Blending (EB) $k-\epsilon$ model relies on the concept of elliptic relaxation that was proposed by [17] for Reynolds-stress models. The initial model required the solution of six additional transport equations, but this number was later reduced to a single additional equation. The model was later simplified by [18] to make it more industry-friendly. The elliptic relaxation model led to the development of some two-equation eddy viscosity models. Significant modifications to this model make it truly robust for complex flow geometries [19]. The EB model accurately models near wall anisotropy and is valid both in the low Reynolds number boundary layer and the high Reynolds number bulk flow. The model is well suited for internal flows, heat transfer modeling, and other cases where accurate near wall modeling is important.

The EB model accurately models near-wall anisotropy and is valid both in the low Reynolds number boundary layer and the high Reynolds number bulk flow. The model is well-suited for internal flows, heat transfer modeling, and other cases where accurate near wall modeling is important [1].

In terms of the comparisons available in the literature, in the document [20], five $k-\epsilon$, two-equation models are studied: the standard $k-\epsilon$ model, a low-Reynolds-number $k-\epsilon$ model, a two-layer $k-\epsilon$ model, a two-scale $k-\epsilon$ model, and a renormalization group (RNG) $k-\epsilon$ model. They are evaluated for their performance in predicting natural

convection, forced convection, and mixed convection in rooms, as well as an impinging jet flow. Corresponding experimental data from the literature are used for validation. It is found that the prediction of the mean velocity is more accurate than that of the turbulent velocity. These models are neither able to predict anisotropic turbulence correctly nor to pick up the secondary recirculation of indoor air flow; otherwise, the performance of the standard $k-\epsilon$ model is good. The RNG $k-\epsilon$ model is slightly better than the standard $k-\epsilon$ model and is therefore recommended for simulations of indoor air flow. The performance of the other models is not stable.

In [21] simulated the wind flow around a high-rise building using different $k-\epsilon$ turbulence models with a polyhedral mesh system. The accuracy of the simulation results was evaluated against the AIJ wind tunnel experiment results. It was concluded that in practice, it is recommended to use the STLKE model to explore high-wind-speed areas around high-rise buildings (e.g., the high-wind-speed areas around buildings during a typhoon, the maximum wind speed area around high-rise buildings, etc).

Given the literature status, there is a lack of knowledge regarding comparing the different cell types in a mesh and the impact of the variations of the $k-\epsilon$ turbulence model. The first concerns the mesh's dominant cell type (hexahedra, tetrahedra, and polyhedral) for a fixed base size. The goal is to provide an initial guideline of what mesh type to use when initiating a study of flow around a complex structure, such as a fuel assembly with a vane-type spacer grid.

The $k-\epsilon$ turbulence model is critically important in CFD simulations due to its robustness, simplicity, and reasonable accuracy across a wide range of turbulent flows. The $k-\epsilon$ model is widely used in both academic research and practical engineering design, contributing significantly to the advancement of fluid dynamics. Additionally, the $k-\epsilon$ turbulence model was adapted for several applications as mentioned previously, and its variations must be assessed to analyze the impact on the results.

Considering this, this article aims to compare the effect of different mesh element types on the results of water flow through a representative spacer grid. Three variations of the $k-\epsilon$ turbulence model available in Simcenter STAR-CCM+ [1] were analyzed along with each dominant mesh element type. The utilized $k-\epsilon$ turbulence models were Standard Two-layer (STL), Realizable Two-Layer (RTL), and Elliptic Blending (EB), while the dominant cell types included cartesian, polyhedral, and tetrahedral shapes.

2. MATERIALS AND METHODS

2.1. Geometry, meshes and boundary conditions

Aiming to compare mesh element types, the numerical and experimental studies by Karoutas et al. [22] were taken as a reference basis to define the boundary conditions and geometry models for the simulations, which were performed using Simcenter STAR-CCM+ [1]. This software conducts CFD analysis by implementing finite volume method to solve the conservation equations for mass, momentum and energy.

Figure 1 depicts the generated geometry composing either a subchannel of a fuel element and also a spacer grid similar in dimensions, measuring planes and boundary conditions as described by [22]. In this figure, eight measurement planes are presented (O-G). Besides the measurement planes, a measurement line was analysed at the center of the left row of subchannels on each plane to evaluate axial and lateral velocities. The channel inlet was set with a flow velocity equal to 6.79 [m/s] and a zero pressure gradient, whereas the end of the channel was defined with zero uniform static pressure. Regarding the spacer grid and walls were assigned with no slip condition. The initial and boundary conditions are presented in Table 1. The performed calculations considered a steady-state simulations with all fluid properties kept constant and isothermal flow.

Using the geometry presented in Figure 1, three meshes were created under the same refinement conditions, changing only the dominant types of elements applied. A quarter of these final meshes are presented in Figure 2. The parameters used for the generation of the meshes are presented in Table 2 as the number of total elements.

Figure 1: Mesh geometry and boundary conditions used in the simulations [mm].

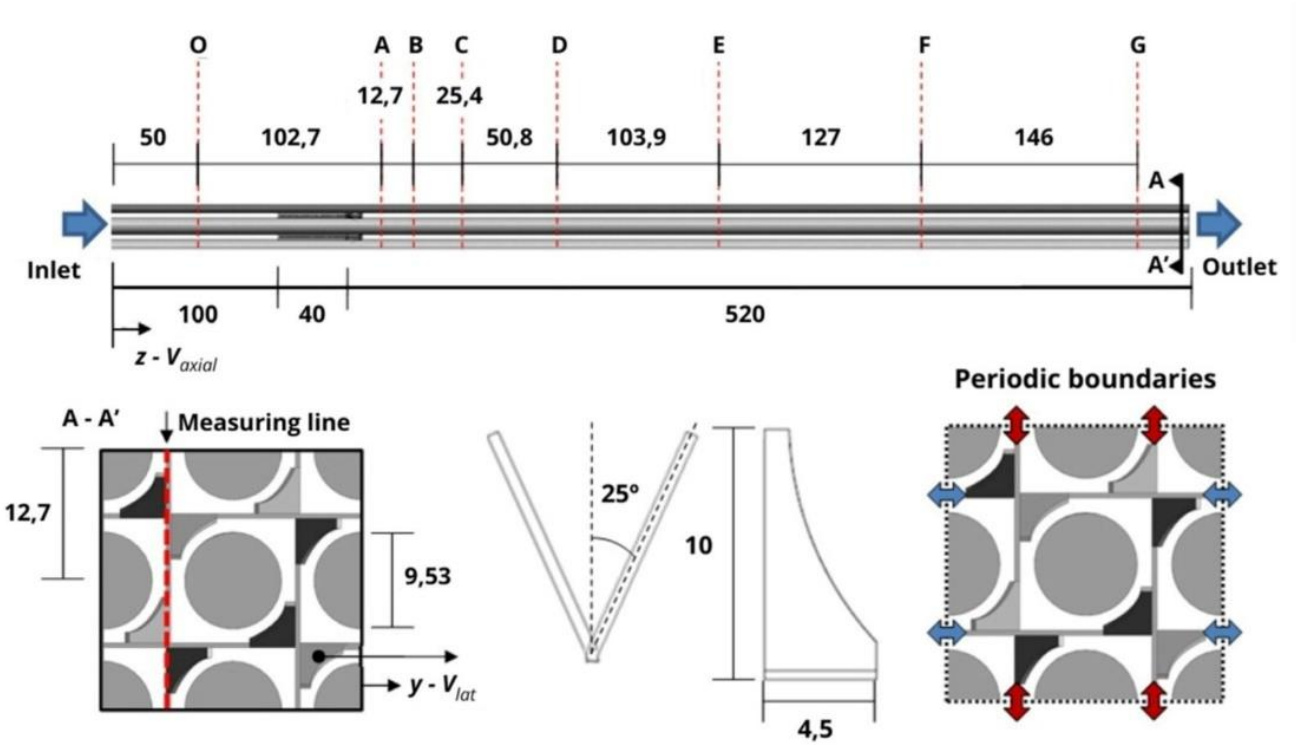

Source: Adapted from [2].

Table 1: Boundary and initial conditions.

BOUNDARY	CONDITION	VALUES
Inlet	Uniform axial velocity	6.79 m/s – 5% turbulence intensity
Outlet	Static pressure	0 Pa
Walls	Smooth non-slip walls	-
Sides	Periodic	-

Figure 2: One quarter of the final meshes generated.

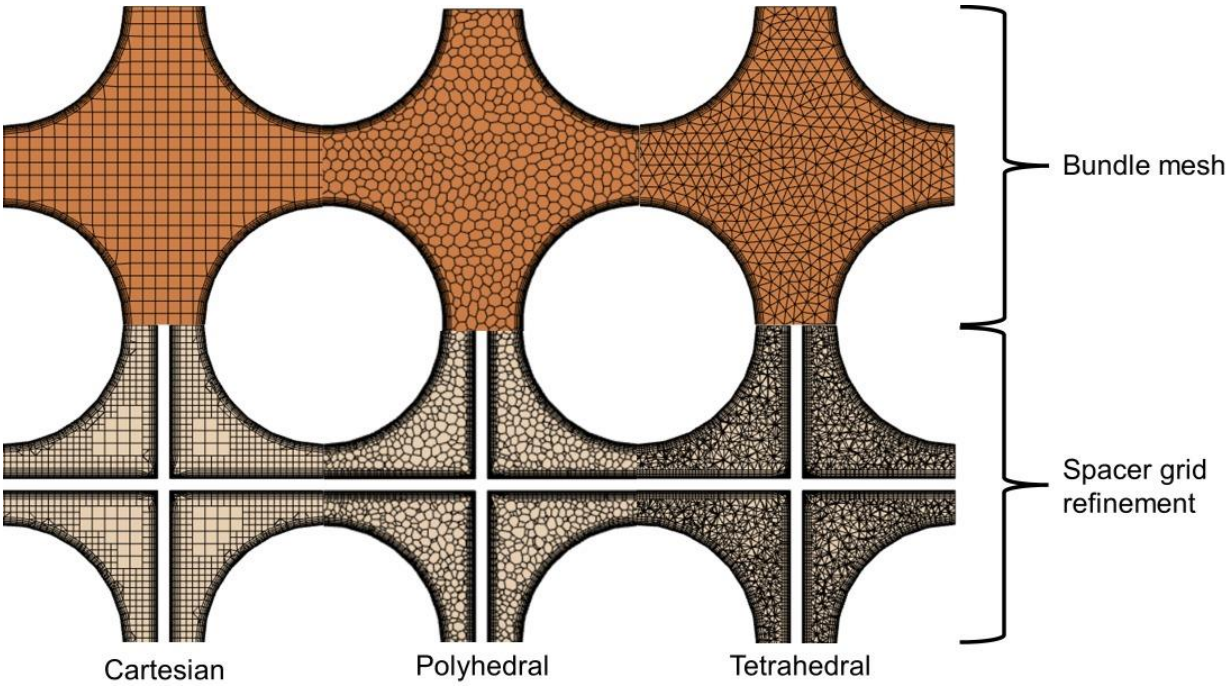

Source: Author.

Table 2: Meshes parameters.

PARAMETERS	CARTESIAN MESH	POLYHEDRAL MESH	TETRAHEDRAL MESH
Base size [m]	5.0E-4	5.0E-4	5.0E-4
Prism layers	6	6	6
Prism layer stretching	1.2	1.2	1.2
Prism layers thickness	3.25E-4	3.25E-4	3.25E-4
Number of cells	6939973	7602176	23611040

3. RESULTS AND DISCUSSIONS

The findings of the present study are organized according to the evaluated variables of interest. Initially, the pressure drop across the modeled domain for the various meshes and $k-\epsilon$ turbulence models assessed is presented. Subsequently, the profiles of lateral and axial velocities are depicted for the same range of simulations conducted. The resultant velocity

vector and vorticity on the first plane post the spacer grid (Plane A) are evaluated for the employed meshes and $k-\epsilon$ turbulence models. Finally, the Secondary Flow (SF) was analyzed for the significant turbulence models and mesh configurations presented in this study.

Figure 3 illustrates the obtained pressure drop behavior for different meshes using the STL $k-\epsilon$ turbulence model. In this figure, all meshes were unable to replicate the values demonstrated by the experiments conducted by [23] and [24]. This could be attributed to the known damping characteristic of the STL $k-\epsilon$ turbulence model. Nevertheless, the results from the simulations showed the same trend as the experiment. Moreover, the numerical uncertainty was not evaluated, which could potentially validate these results if all values fall within the range of confidence intervals. From these results, the STL $k-\epsilon$ model appears to be a secondary choice due to the overestimation of pressure loss across the domain.

Figure 3: Pressure drop comparison between experiment and different numerical simulations using STL $k-\epsilon$ turbulence model.

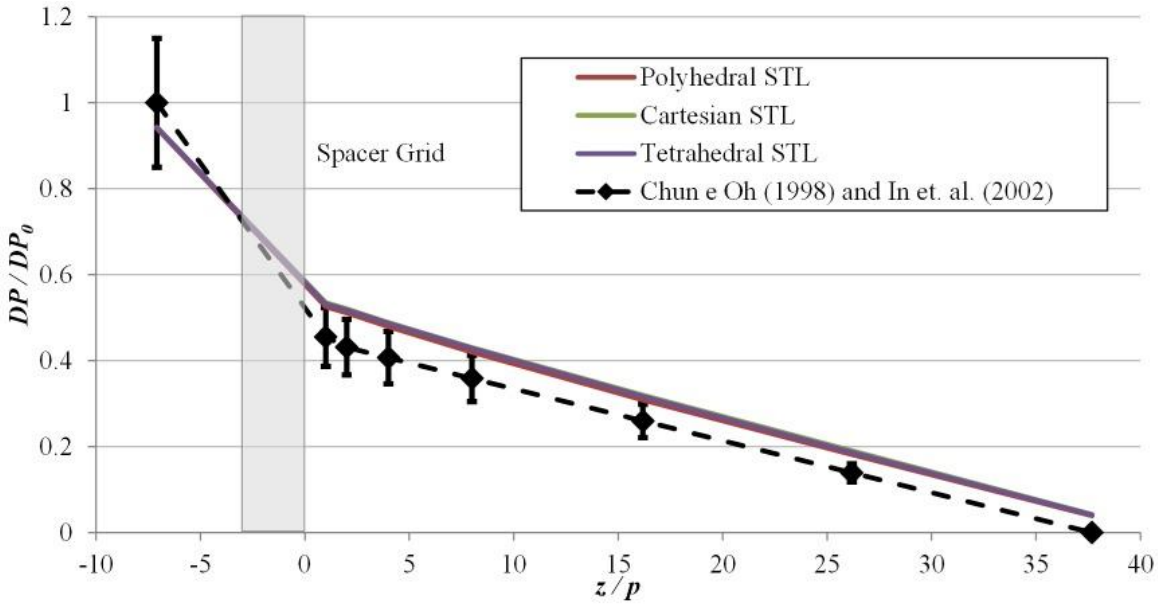

Source: Author.

Figure 4 depicts the obtained pressure drop behavior for different meshes using the RTL $k-\epsilon$ turbulence model. In this figure, the models employing a mesh based on polyhedral and tetrahedral cells successfully adhered to the experimental results within the uncertainty range.

Solely the model using Cartesian cells was unsuccessful in predicting the pressure loss subsequent to the spacer grid. However, similar to the behavior shown in Figure 3, all models demonstrated the same trend exhibited by the experimental results. These findings indicate that the numerical diffusion induced by the Cartesian mesh predominates over the effect of the turbulent model, as the Cartesian mesh essentially displayed identical results in Figures 3 and 4.

Figure 4: Pressure drop comparison between experiment and different numerical simulations using RTL $k-\epsilon$ turbulence model.

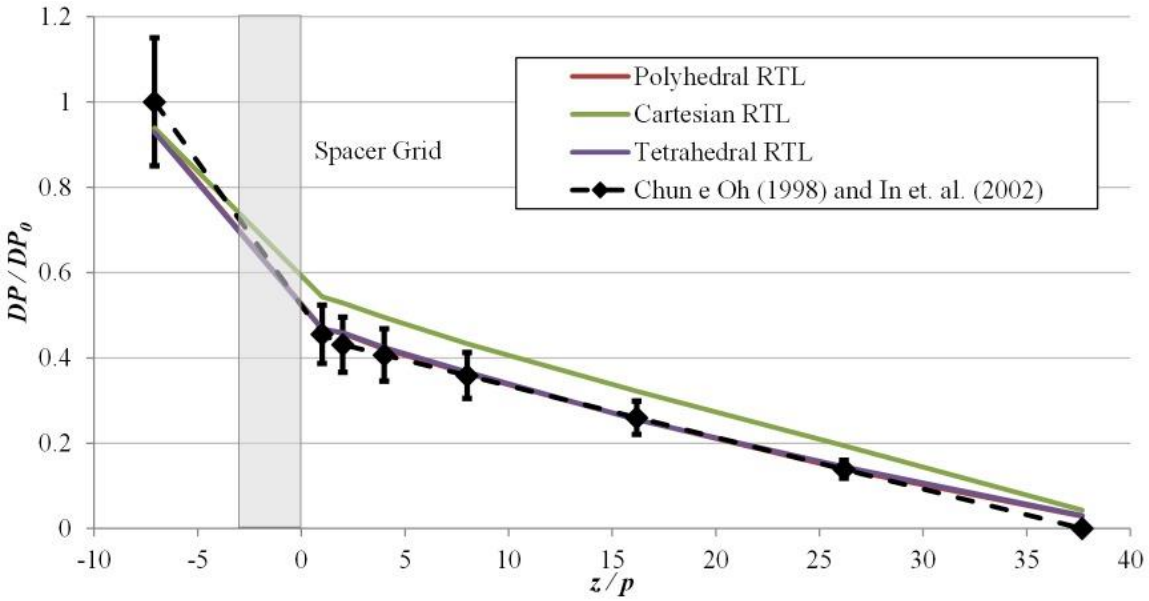

Source: Author.

Finally, Figure 5 depicts the obtained pressure drop behavior for different meshes using the EB $k-\epsilon$ turbulence model. For this particular configuration combination, only the Polyhedral mesh was successful in capturing the pressure loss across the domain. The Cartesian and Tetrahedral meshes overestimated the pressure loss subsequent to the spacer grid. The behavior of the Tetrahedral mesh is unexpected, given that this type of mesh is usually suitable for avoiding numerical diffusion. However, all models managed to capture the trend of pressure loss, and an evaluation of the numerical uncertainty could potentially align the results.

In relation to the results for pressure loss across the domain, the Polyhedral mesh model appeared to emulate the experimental behavior, with the exception of the STL $k-\epsilon$ turbulence model. Furthermore, the Tetrahedral mesh was unsuccessful for the STL $k-\epsilon$ and EB $k-\epsilon$ turbulence models, while the Cartesian mesh was ineffective for all tested $k-\epsilon$ models.

Figure 5: Pressure drop comparison between experiment and different numerical simulations using EB $k-\epsilon$ turbulence model.

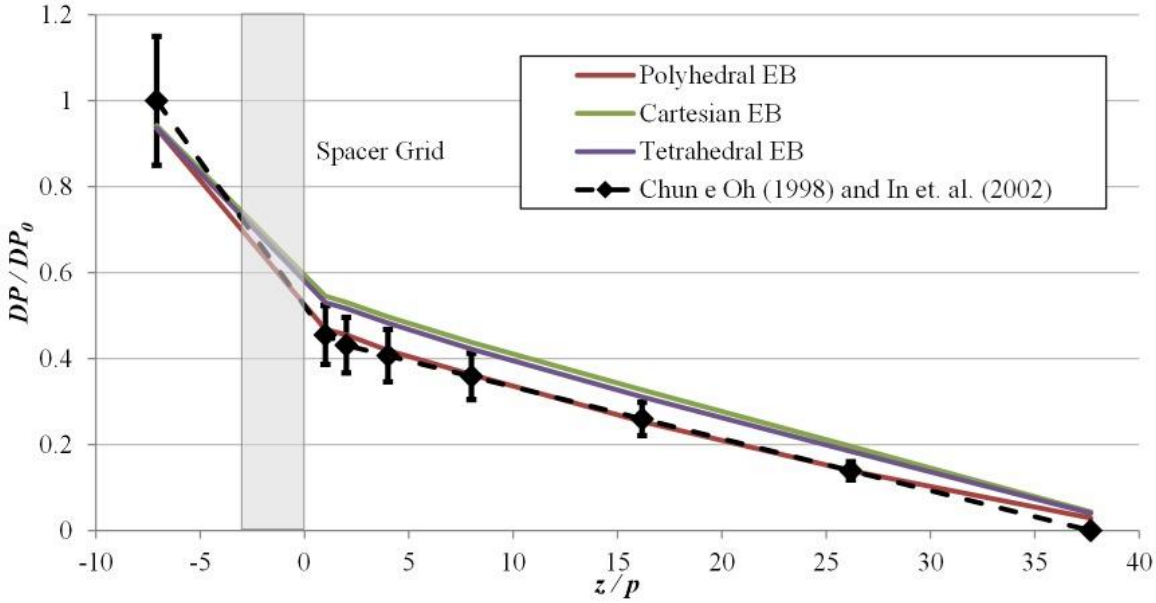

Source: Author.

Figure 6 depicts the lateral velocity outcomes of the different meshes for the STL $k-\epsilon$ turbulence model. Only Planes A, D, and G are displayed, but the intermediate planes exhibited intermediate results in terms of magnitudes between these planes. This was observed for all evaluated velocity results (axial and lateral). In Figure 6, the employed models demonstrated a behavior similar to the experiment for Plane A, although with a displacement on the evaluated length. This could be attributed to a misalignment in the experimental bench, given that the CFD are perfectly orthogonal. For Plane D, the models captured the peaks and valleys of the curve in a with reduced magnitude, indicating turbulence damping. This damping is further amplified in Plane G results, which displayed almost no lateral velocity for the evaluated models.

Figure 6: Lateral velocity comparison between experiment and different numerical simulations using STL $k-\epsilon$ turbulence model.

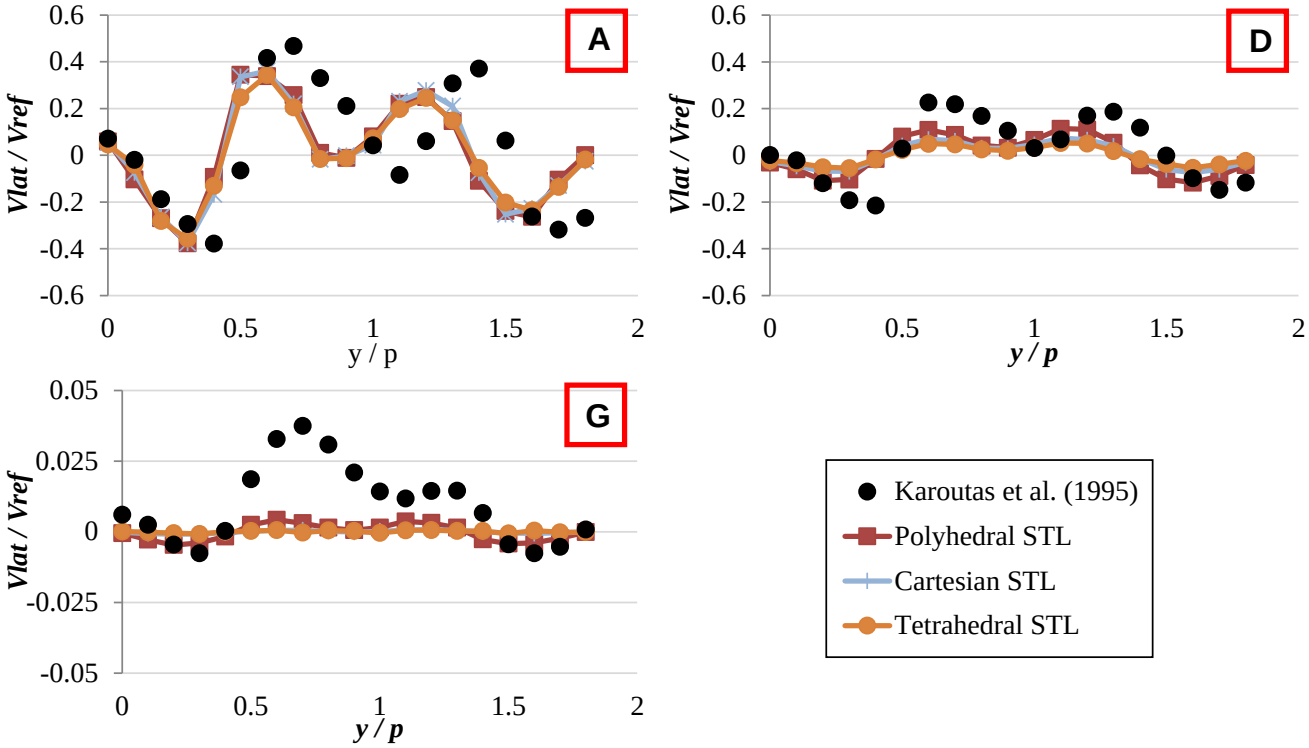

Source: Author.

Figure 7 presents the axial velocity outcomes of the various meshes for the STL $k-\epsilon$ turbulence model. The models were unsuccessful in capturing the experimental behavior for Plane A. This was anticipated based on the findings of [2]. The replication of results for axial velocity on Plane A appears to be challenging due to the internal components of the grids that are not accountable due to the lack of available data on the original work [22]. The employed models demonstrated the trends of the experiment for Planes D and G. However, there is a slight overestimation of the axial velocity for Plane D. This effect is magnified for Plane G.

Figure 7: Axial velocity comparison between experiment and different numerical simulations using STL $k-\epsilon$ turbulence model.

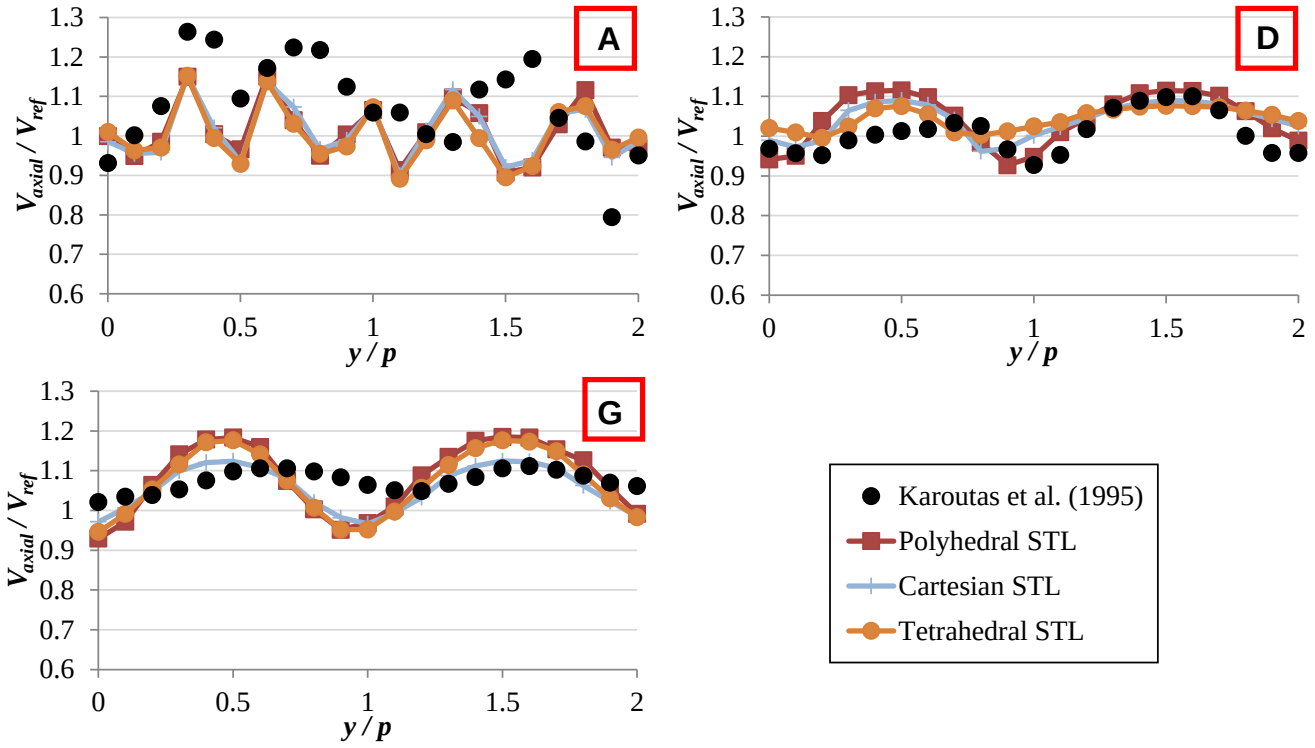

Source: Author.

Figure 8 illustrates the lateral velocity outcomes of the various meshes for the RTL $k-\epsilon$ turbulence model. This figure reveals that the developed models were successful in capturing the experimental behavior for Planes A and D, albeit with a displacement. As previously affirmed, this displacement could be attributed to misalignment on the experimental bench. For Plane G, all models were unsuccessful in capturing the amplitudes of the experiment. All models exhibited a symmetrical behavior. The Polyhedral and Tetrahedral meshes overestimated the amplitudes of the lateral velocity, particularly for the negative values. Conversely, the Cartesian mesh underestimated it.

Figure 8: Lateral velocity comparison between experiment and different numerical simulations using RTL $k-\epsilon$ turbulence model.

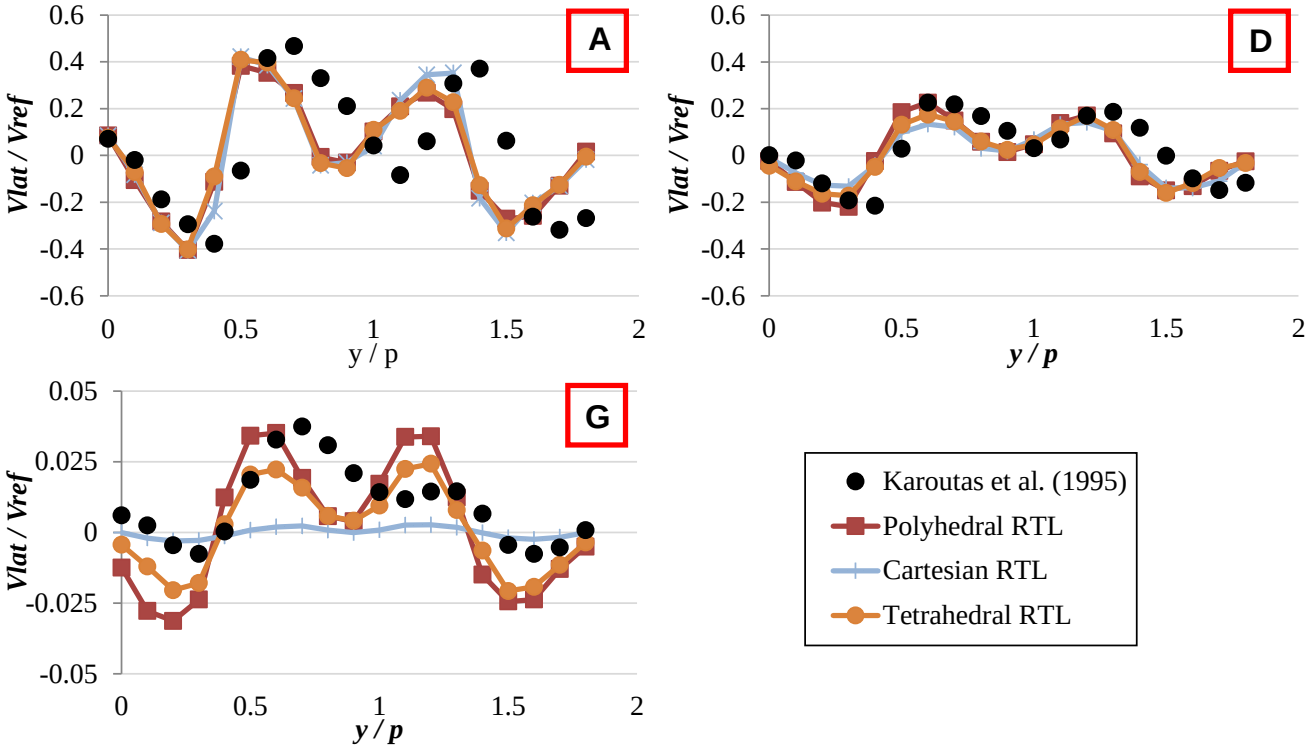

Source: Author.

Figure 9 presents the axial velocity outcomes of the different meshes for the RTL $k-\epsilon$ turbulence model. As previously stated, the replication of Plane A for axial velocity presents a significant challenge. For Planes D and G, the developed models successfully reproduced the experimental trend, albeit with an overestimation of the magnitudes at the valleys and peaks of the curves. The performance of the models developed using the RTL $k-\epsilon$ turbulence model exhibited similar results when compared to that of the STL $k-\epsilon$ turbulence model in terms of axial velocity. Once again, the Cartesian mesh displayed reduced values for Plane G. This is an indication of the numerical diffusion brought about by hexahedral cells not aligned with the flow, which is the case close to the spacer grid. This misalignment drags the numerical diffusion forward away from the spacer grid.

Figure 9: Axial velocity comparison between experiment and different numerical simulations using RTL $k-\epsilon$ turbulence model.

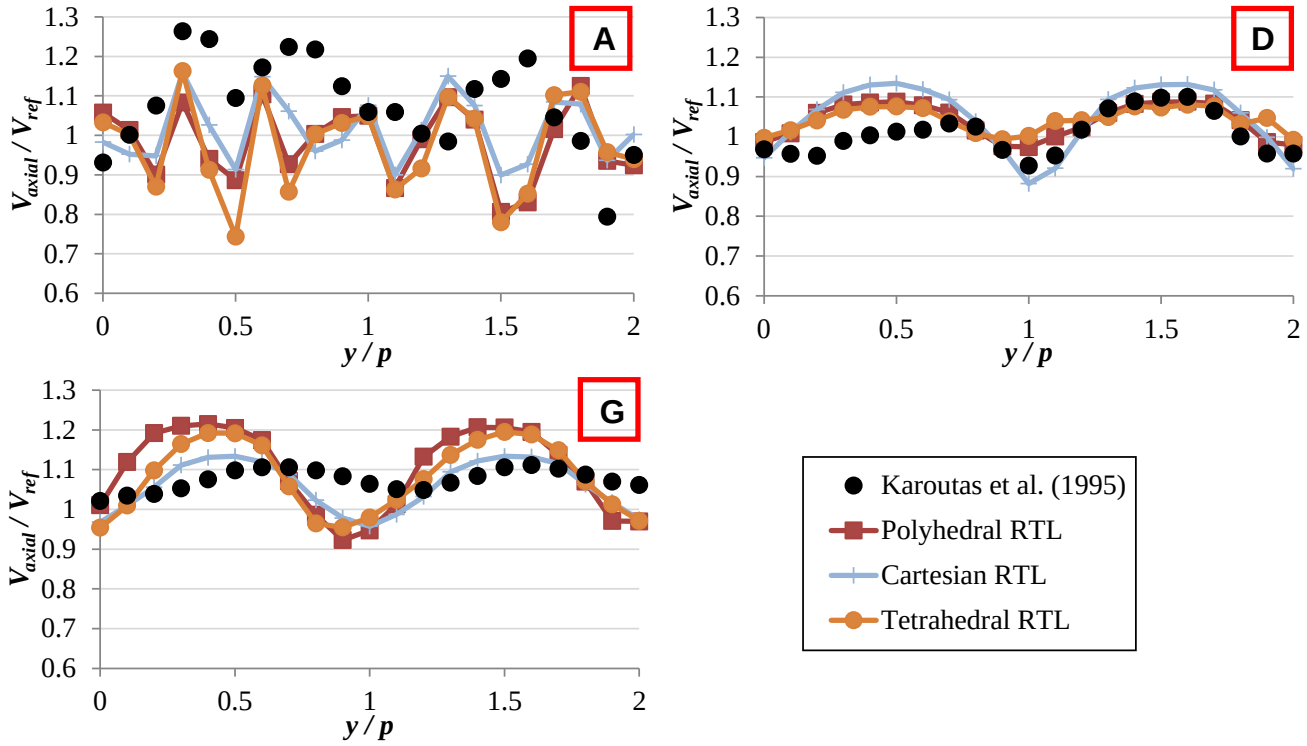

Source: Author.

Figure 10 presents the lateral velocity outcomes of the various meshes for the EB $k-\epsilon$ turbulence model. Similar to the other turbulence models, there is a slight displacement between the experimental data and the obtained results. For Planes A and D, all developed models successfully replicated the experimental behavior in terms of curve amplitudes. For Plane G, the Polyhedral mesh overestimated the lateral velocity, while the Cartesian and Tetrahedral meshes underestimated it.

Figure 10: Lateral velocity comparison between experiment and different numerical simulations using EB $k-\epsilon$ turbulence model.

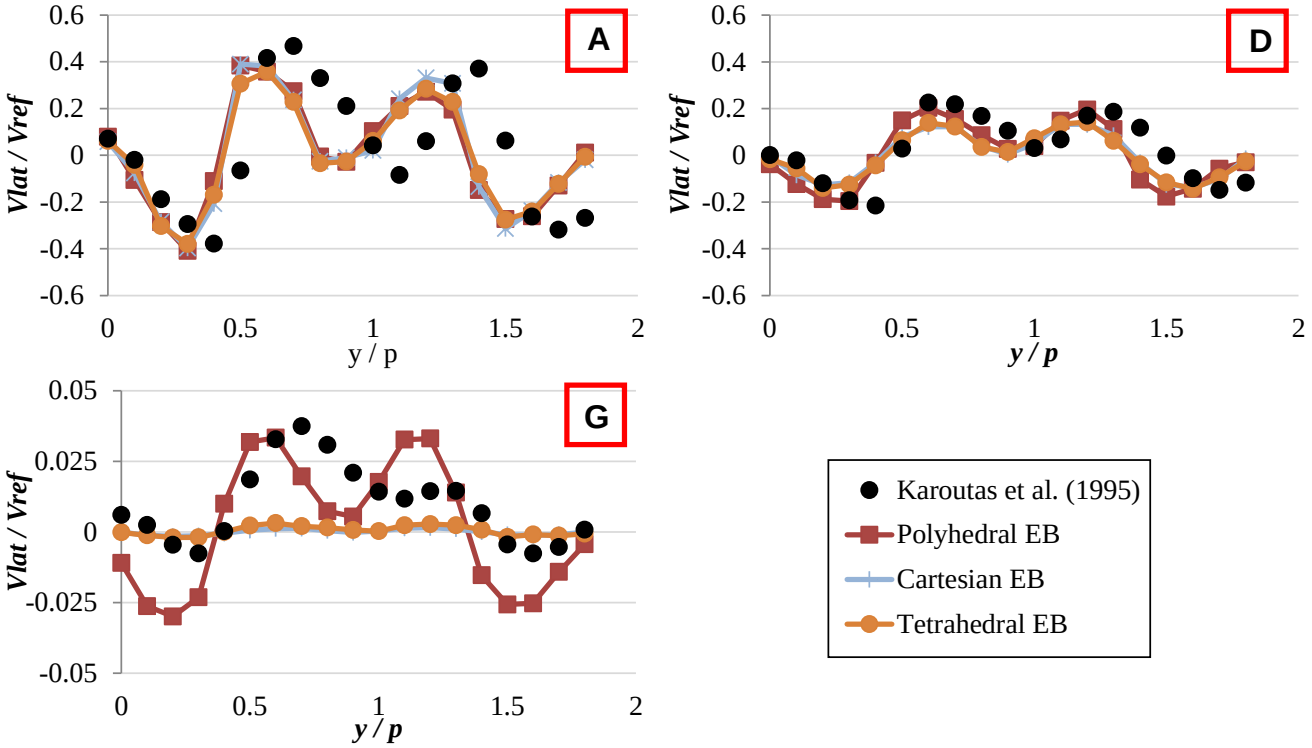

Source: Author.

With respect to the lateral velocity for all the developed models, the Polyhedral mesh demonstrated a consistency of results. The overestimation of the results for Plane G could potentially be attributed to the absence of internal structural components that were present in the experiment. The Tetrahedral mesh also exhibited a reasonable concurrence, although with a mesh nearly three times larger.

Figure 11 presents the axial velocity outcomes of the various meshes for the EB $k-\epsilon$ turbulence model. As previously stated, the replication of Plane A for axial velocity poses a significant challenge. The models developed for Planes D and G successfully encapsulated the experimental trend, albeit with an overestimation of the magnitudes at the valleys and peaks of the curves. The performance of the models developed utilizing the EB $k-\epsilon$ turbulence model mirrored that of the STL and RTL $k-\epsilon$ turbulence models in terms of

axial velocity. Moreover, the Cartesian mesh displayed diminished values for Plane G, indicative of the numerical diffusion induced by hexahedral cells not aligned with the flow.

Figure 11: Axial velocity comparison between experiment and different numerical simulations using EB $k-\epsilon$ turbulence model.

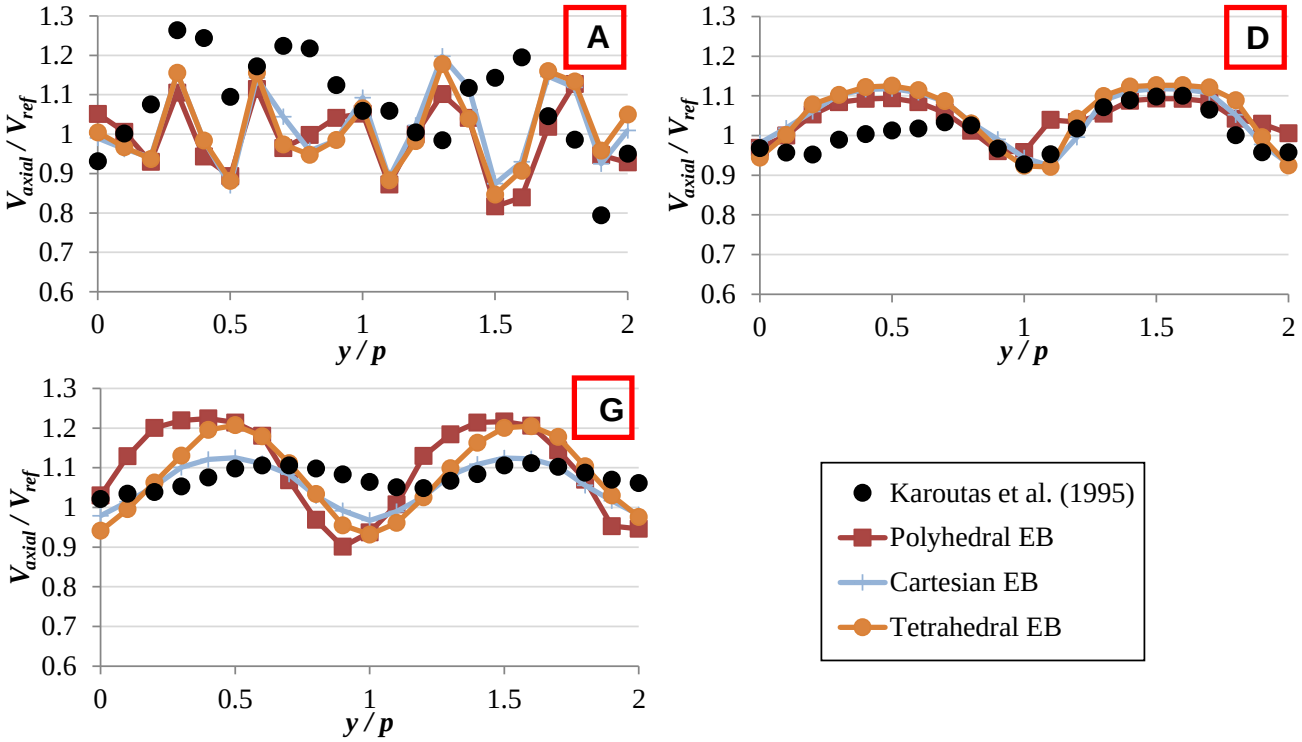

Source: Author.

Figure 12 presents the outcomes for velocity and vorticity on Plane A of the various meshes for the STL $k-\epsilon$ turbulence model. Across all meshes, the velocity magnitudes exhibited similarity, with the Cartesian and Tetrahedral meshes displaying lower velocities at the centers of the subchannels. The developed models also demonstrated uniformity amongst each other in terms of vorticity. The areas of low velocity are associated with the higher vortices. The behaviors of velocity and vorticity were in alignment with observations in the literature [2], characterized by high recirculation within the subchannel (swirl), as opposed to crossflow. For Plane A, the turbulence model held dominance over the mesh, which is consistent with the results of lateral and axial velocities (refer to Figures 6 and 7).

Figure 12: Velocity and vorticity comparisons between different meshes using STL $k-\epsilon$ turbulence model on Plane A.

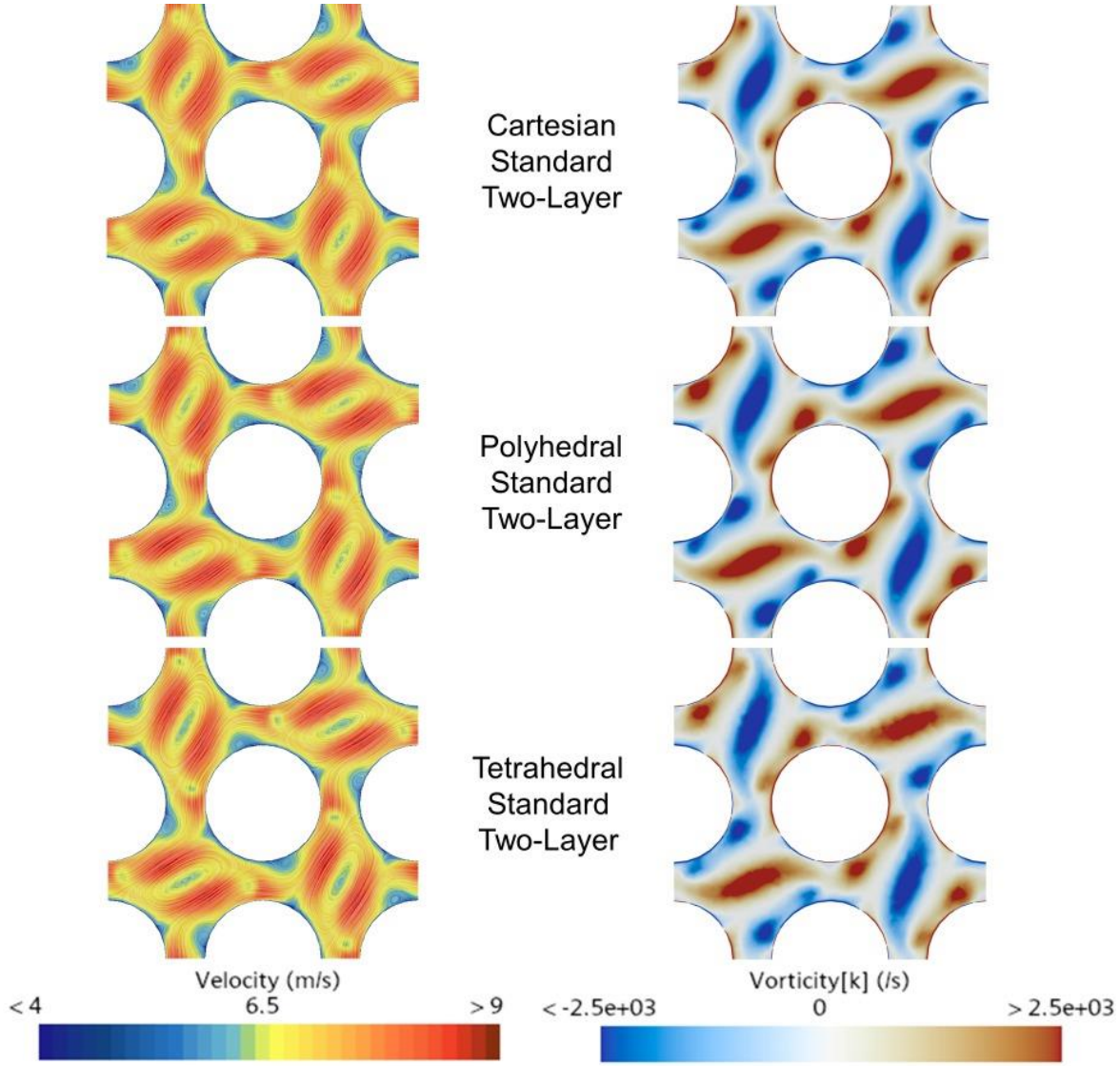

Source: Author.

Figure 13 presents the outcomes for velocity and vorticity on Plane A of the various meshes for the RTL $k-\epsilon$ turbulence model. In this instance, the type of mesh exhibited a significant impact on the velocity profile, although this was not captured by the measurements taken along the probe line (refer to Figures 8 and 9). The velocity recirculation was dampened by the Cartesian mesh, while it was progressively amplified by the Polyhedral and Tetrahedral meshes, in that sequence. In terms of vorticity, the effects of velocity can be

observed in the secondary vortices close to the walls, where the Polyhedral and Tetrahedral meshes displayed more intense vortices.

Figure 13: Velocity and vorticity comparisons between different meshes utilizing RTL $k-\epsilon$ turbulence model on Plane A.

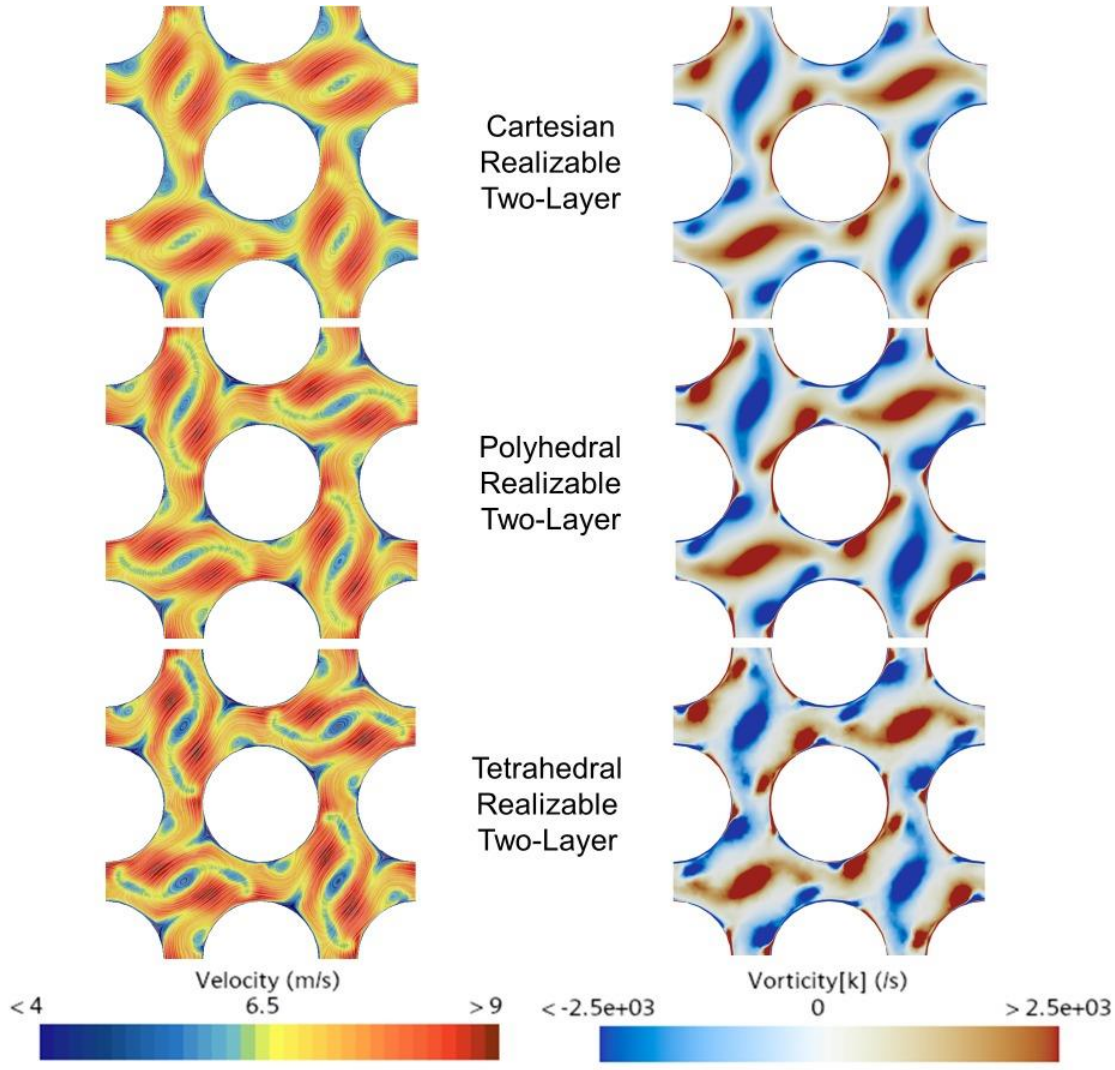

Source: Author.

Figure 14 presents the outcomes for velocity and vorticity on Plane A of the various meshes for the EB $k-\epsilon$ turbulence model. In this illustration, the impact of the mesh on the velocity profile is less pronounced than for the RTL $k-\epsilon$ turbulence model. Nonetheless, the three mesh models exhibited some distinct characteristics. The Cartesian mesh displayed

a more circular recirculation spot at the center of the subchannels. The Polyhedral mesh demonstrated greater smoothness between the recirculation and the high-velocity spots. On the other hand, the Tetrahedral mesh exhibited a steeper gradient between the locations of low and high velocity. In terms of vorticity, the Cartesian and Tetrahedral meshes displayed more concentrated secondary vortices.

Figure 14: Velocity and vorticity comparisons between different meshes utilizing EB $k-\epsilon$ turbulence model on Plane A.

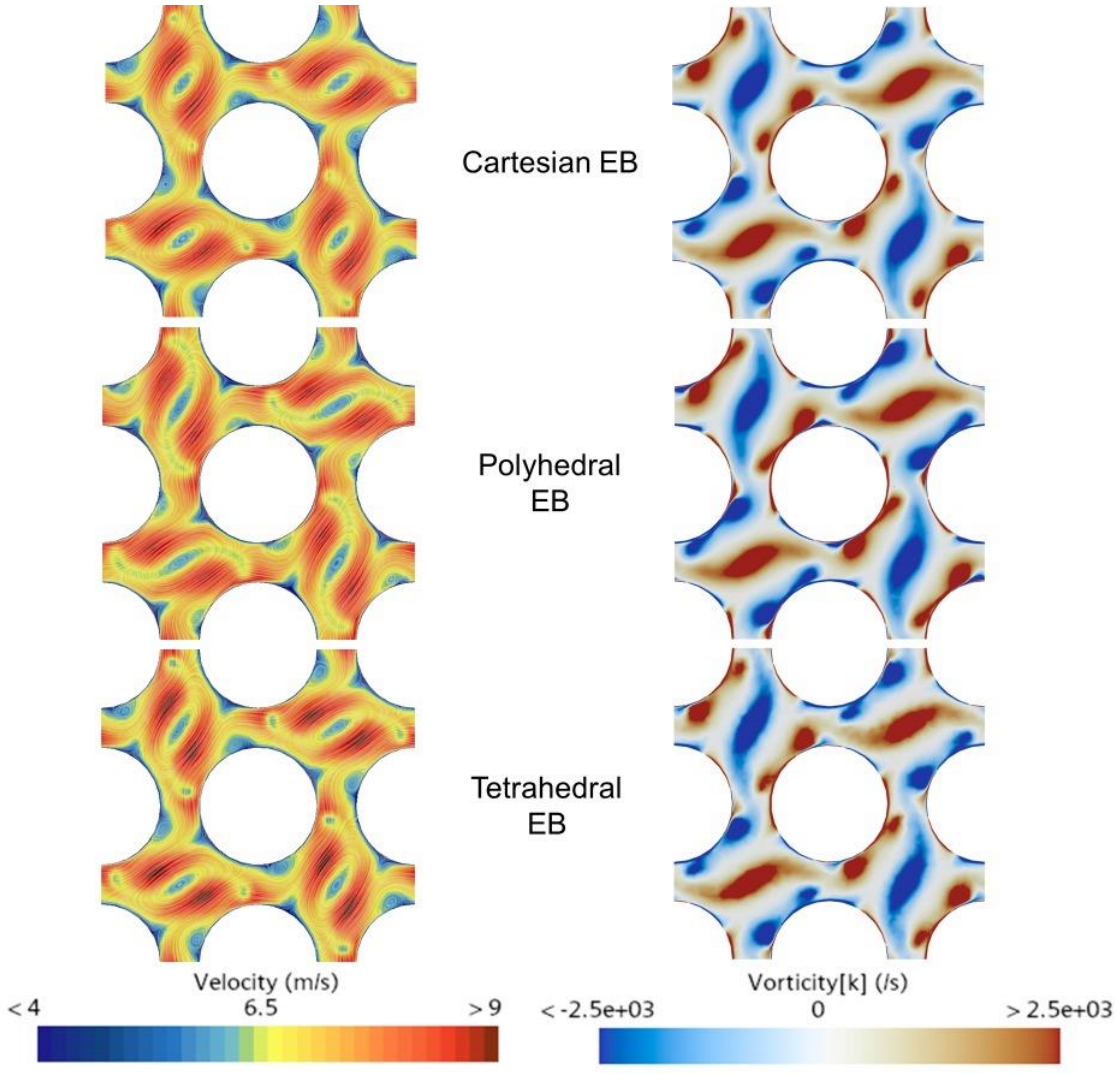

Source: Author.

Figure 15: Secondary Flow (SF) for all the achieved results.

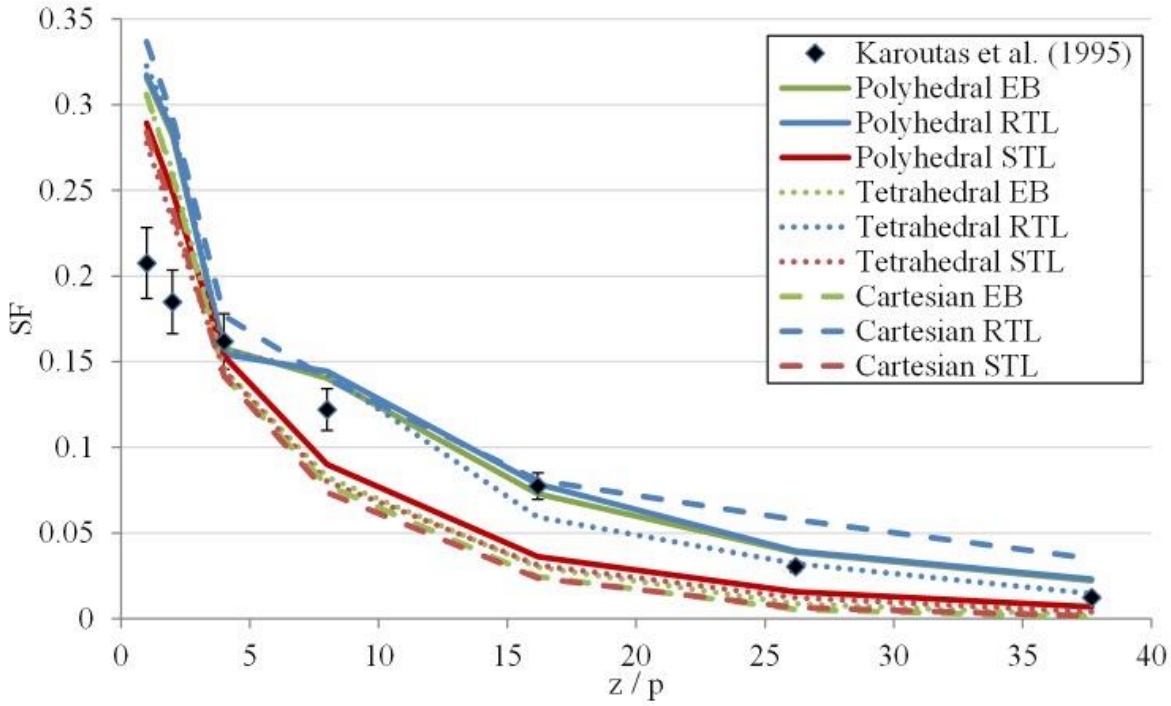

Source: Author.

Figure 15 presents the secondary flow results for the relevant meshes and turbulence models at 7 positions downstream of the spacer grid, highlighting some of their specific characteristics. All models initially exhibited values higher than the experimental data. Among them, the Polyhedral STL, Tetrahedral STL, Cartesian STL, and Cartesian EB models showed a rapid decrease near the grid, describing smooth curves but with lower magnitudes compared to the other models. The Polyhedral EB and RTL models displayed agreement with each other and with the experimental data, except at positions closer to the grid. An anomalous behavior was observed between heights 3 and 4, indicating a turbulence effect. The Cartesian RTL model exhibited slightly higher values, particularly at positions farther from the grid. However, all models demonstrated a consistent trend of reducing intensity downstream spacer grid.

4. CONCLUSIONS

This study conducted a comparative analysis of the results derived from simulations of water flow through spacer grids of nuclear fuel elements, varying mesh elements, turbulence models, and experimental studies. The meshes were constructed with an identical level of refinement, with only the type of element used being altered, while the boundary conditions and standard parameters employed for the simulations remained the same. It is noteworthy from the results that, under the conditions imposed on the simulations, the Polyhedral mesh element is the most suitable. It offers the best cost-benefit ratio when considering the computational cost, as it comprises fewer elements than the Tetrahedral one, and it demonstrates commendable accuracy of the results in comparison to the experimental studies. In relation to the Cartesian mesh, the results exhibit more significant discrepancies in relation to the experimental studies.

With respect to the turbulence models, three variations of the $k-\epsilon$ model were evaluated (STL, RTL, and EB). The RTL and EB models fitted more appropriately the experimental results concerning the velocity profiles (lateral and axial). The STL $k-\epsilon$ model dampened the lateral velocity in a more pronounced manner. The pressure drop was not accurately captured by the STL model. For the RTL model, only the Cartesian mesh failed to capture the pressure loss, and for the EB model, only the Polyhedral mesh aligned with the experimental result.

In terms of velocity magnitude and vorticity, the STL models demonstrated similar behavior for all meshes, dampening the velocities. For the RTL and EB models, the mesh exhibited a higher impact on velocity profiles, leading to differences in the secondary recirculation spots presented on vorticity profiles.

The SF evaluated for the primary turbulence models and meshes presented in this study demonstrated consistency, showing a tendency to decrease in intensity downstream of

the spacer grid. Among the models analyzed, the Polyhedral EB, RTL, and Tetrahedral RTL models exhibited the closest agreement with the experimental results.

For future endeavors, more refined meshes should be evaluated, particularly for the Polyhedral model using RTL and EB $k-\epsilon$ models. Potentially, reaching the Large Eddy Simulation (LES) level could lead to the capture of more accurate results. Additionally, numerical uncertainty must be assessed to better comprehend the fit of the numerical results to the experimental ones.

ACKNOWLEDGMENT

The authors are grateful to Brazilian research funding agencies CNEN – Comissão Nacional de Energia Nuclear, CNPq – Conselho Nacional de Desenvolvimento Científico e Tecnológico, CAPES – Coordenação de Aperfeiçoamento de Pessoal de Nível Superior, FAPEMIG – Fundação de Amparo à Pesquisa do Estado de Minas Gerais and FINEP – Financiadora de Estudos e Projetos for the support.

CONFLICT OF INTEREST

All authors declare that they have no conflicts of interest.

REFERENCES

[1] Siemens Digital Industries Software. Simcenter STAR-CCM+ User Manual. Disponível em: https://plm.sw.siemens.com/en-US/simcenter/fluids-thermal-simulation/star-ccm/. Acesso em: 2024.

[2] SANTOS, A. A. C. Investigação numérica e experimental do escoamento de água em feixe de varetas representativo de elementos combustíveis nucleares de reatores do tipo PWR. **PhD Dissertation**. Universidade Federal de Minas Gerais, Belo Horizonte, 2012.

[3] NAVARRO, M. A.; SANTOS, A. A. Evaluation of a numeric procedure for flow simulation of a 5x5 PWR rod bundle with a mixing vane spacer. **Progress in Nuclear Energy**, v. 53, p. 1190-1196, 2011.

[4] IKEDA, K. CFD application to advanced design for high efficiency spacer grid. **Nuclear Engineering and Design**, v. 279, p. 73-82, 2014.

[5] PODILA, K.; RAO, Y.; KRAUSE, M.; BAILEY, J. A CFD simulation of 5x5 rod bundles with split-type spacers. **Progress in Nuclear Energy**, v. 70, p. 167-175, 2014.

[6] CHEN, X.; DU, S.; ZHANG, Y.; YU, H.; LI, S.; PENG, H.; WANG, W.; ZENG, W. Validation of CFD analysis for rod bundle flow test with vaned spacer grids. **Annals of Nuclear Energy**, v. 109, p. 370-379, 2017.

[7] WANG, M.; JU, H.; WU, J.; QIU, H.; LIU, K.; TIAN, W.; SU, G. A review of CFD studies on thermal hydraulic analysis of coolant flow through fuel rod bundles in nuclear reactor. **Progress in Nuclear Energy**, v. 171, 2024.

[8] NAVARRO, M. A.; SANTOS, A. A. Numerical evaluation of flow through a 5x5 PWR rod bundle: effect of the vane arrangement in a spacer grid. In: PROCEEDINGS OF THE INTERNATIONAL NUCLEAR ATLANTIC CONFERENCE (INAC), 2009, Rio de Janeiro, Rio de Janeiro, Brazil. **Numerical evaluation of flow through a 5x5 PWR rod bundle: effect of the vane arrangement in a spacer grid**. Rio de Janeiro, Rio de Janeiro, Brazil: INAC, 2009.

[9] SANTOS, A. A.; BARROS FILHO, J. A.; NAVARRO, M. A. Verification and validation of a numeric procedure for flow simulation of a 2x2 PWR rod bundle. *In*: PROCEEDINGS OF THE INTERNATIONAL NUCLEAR ATLANTIC CONFERENCE (INAC), 2011, Belo Horizonte, Minas Gerais, Brazil. **Verification and validation of a numeric procedure for flow simulation of a 2x2 PWR rod bundle**. Belo Horizonte, Minas Gerais, Brazil: INAC, 2011.

[10] WANG, W.; CAO, Y.; OKAZE, T. Comparison of hexahedral, tetrahedral and polyhedral cells for reproducing the wind field around an isolated building by LES. **Building and Environment**, v. 195, 2021.

[11] HEFNY, M. M.; OOKA, R. CFD analysis of pollutant dispersion around buildings: Effect of cell geometry. **Building and Environment**, v. 44, p. 1699-1706, 2009.

[12] CINOSI, N.; WALKER, S.; BLUCK, M.; ISSA, R. CFD Simulation of turbulent flow in a rod bundle with spacer grids (matis-h) using STAR-CCM+. **Nuclear Engineering and Design**, v. 279, p. 37-49, 2014.

[13] XIONG, J.; LU, C.; QU, W. Validation for CFD simulation in rod bundles with split-vane spacer grids based on LDA measurement. **Frontiers in Energy Research**, v. 8, p. 43, 2020.

[14] JONES, W. P.; LAUNDER, B. E. The prediction of laminarization with a two-equation model of turbulence. **International journal of heat and mass transfer**, v. 15, p. 301-314, 1972.

[15] RODI, W. Experience with two-layer models combining the k-epsilon model with a one-equation model near the wall. *In*: 29th Aerospace sciences meeting, January 1991, Reno, NV, USA. INAC. Reno, NV, USA: AIAA, 1991.

[16] SHIH, T.-H.; LIOU, W. W.; SHABBIR, A.; YANG, Z.; ZHU, J. A new k-eddy viscosity model for high Reynolds number turbulent flows. **Computer & fluids**, v. 24, p. 227-238, 1995.

[17] DURBIN, P. A reynolds stress model for near-wall turbulence. **Journal of Fluid Mechanics**, v. 249, p. 465-498, 1993.

[18] MANCEAU, R.; HANJALI'C, K. Elliptic blending model: A new near-wall reynolds-stress turbulence closure. **Physics of Fluids**, v. 14, p. 744-754, 2002.

[19] BILLARD, F.; LAURENCE, D. A robust k- ε- v2/k elliptic blending turbulence model applied to near-wall, separated and buoyant flows. **International Journal of Heat and Fluid Flow**, v. 33, p. 45-58, 2012.

[20] CHEN, QINGYAN. "Comparison of different k-ε models for indoor air flow computations." **Numerical Heat Transfer, Part B Fundamentals**, v. 28, p. 353-369, 1995.

[21] XIONG, M., CHEN, B., ZHANG, H. and QIAN, Y. Study on accuracy of cfd simulations of wind environment around high-rise buildings: a comparative study of k-ε turbulence models based on polyhedral meshes and wind tunnel experiments, **Applied Sciences**, v. 12, p. 7105, 2022.

[22] KAROUTAS, Z.; GU, C.-Y.; SCHÖLIN, B. 3-D flow analyses for design of nuclear fuel spacer. *In*: PROCEEDINGS OF THE US NUCLEAR REGULATORY COMMISSION (NRC), 10-15 September 1995, Saratoga Springs, NY, USA. 3-D flow

analyses for design of nuclear fuel spacer. Saratoga Springs, NY, USA: US Nuclear Regulatory Commission, 1995.

[23] CHUN, T.-H.; OH, D.-S. A pressure drop model for spacer grids with and without flow mixing vanes. **Journal of Nuclear Science and Technology**, v. 35, p. 508-510, 1998.

[24] IN, W. K.; OH, D. S.; CHUN, T. H. Empirical and computational pressure drop correlations for pressurized water reactor fuel spacer grids. **Nuclear techonology**, v. 139, p. 72-79, 2002.

LICENSE